Heteroepitaxy of GaP on Si(100)*

K. J. Bachmann,[a),b),d)] U. Rossow,[c)] N. Sukidi,[b)] H. Castleberry,[b)] and N. Dietz[a),c)]

North Carolina State University, Raleigh, North Carolina 27696-7919

In this article, we analyze the kinetics of heteroepitaxial growth of GaP on Si(100) by pulsed chemical beam epitaxy on the basis of results obtained by real-time optical process monitoring. In view of the large barrier to epitaxial growth on oxygen or carbon contaminated silicon surface elements and the low stacking fault energy for GaP, residual contamination of the silicon surface contributes to defect formation in the initial phase of GaP heteroepitaxy on Si, and requires special measures, such as surface structuring, to limit the propagation of defects into the epitaxial film. The control of the supersaturation during the first 10–20 s of film formation is essential for the quality of subsequent epitaxial growth and is limited to a narrow process window between three-dimensional nucleation and overgrowth at low Ga supersaturation and gallium-cluster formation at high Ga supersaturation. Steady state heteroepitaxial growth is described by a four-layer stack substrate/epilayer/surface reaction layer (SRL)/ambient and, depending of the source vapor flux, allows for more than monolayer coverage. Under this special condition of low-temperature CBE, the kinetics of chemical reactions in the SRL is composed of homogeneous reactions creating/consuming intermediates that participate in surface reactions including the incorporation of Ga and P atoms into the epitaxial film. For the homogeneous part of the surface kinetics the dipole approximation provides an adequate correlation of the changes in the dielectric function of the SRL to the activities of randomly distributed reactants and products. No adequate correlation of the dielectric function exists to the concentrations of strongly bonded surface atoms and surface molecules. Therefore, quantitative assessments of the heterogeneous kinetics on the crystal surface cannot use real-time optical monitoring as a reliable basis. © 1996 American Vacuum Society.

I. INTRODUCTION

Research concerning polar-on-nonpolar heterostructures has been motivated for more than a decade by potential technological applications and scientific questions of general importance. However, progress with regard to both technological and scientific goals has been slow. The primary reasons for this are as follows.

(1) The formation of defects during early stages of nucleation and heteroepitaxial overgrowth and their propagation into the epitaxial film.

(2) The roughening of the surface of the epilayer in the course of epitaxial growth, complicating the modeling and control of the kinetics of heteroepitaxial growth.

(3) Interface broadening related to surface reactions, reconstruction and interdiffusion.

As discussed in Sec. III in more detail, these three problem areas are linked, so that their separation and control provides for a considerable challenge. Here we focus onto GaP heteroepitaxy on Si(100) by pulsed chemical beam epitaxy.

II. EXPERIMENT

Figures 1(a) and 1(b) show schematic representations of the experimental arrangement for pulsed CBE.[1] Pulsed ballistic beams of the source vapors, e.g., tertiary-butylphosphine (TBP) and triethylgallium (TEG) for the growth of GaP, are directed onto a substrate wafer, e.g., a silicon wafer that is heated from the back. For real-time monitoring of the kinetics of heteroepitaxy, we combine several supplementing nonintrusive optical techniques, such as p-polarized reflectance spectroscopy (PRS),[2] reflectance difference spectroscopy (RDS),[3] and laser light scattering (LLS). In addition, reflected high energy electron diffraction (RHEED) and mass spectrometric sampling are available on the system. Here we focus onto results of single-wavelength PRS and LLS. A comparison of these techniques to RDS is provided in our companion article.[4] PRS is based on the changes in the reflectivity during the formation of a heteroepitaxial stack with regard to a chopped beam of p-polarized laser light of below band gap energy that impinges onto the surface at the Brewster angle of the substrate. For monitoring of GaP heteroepitaxy on silicon, we use HeNe laser radiation at 632.8 nm wavelength, polarized by a Glan–Thompson polarizer to a ratio of the s- and p-polarized components of the incident intensity $I_s/I_p \approx 10^{-6}$. This corresponds to a residual reflectivity of the Si surface of the order of 10^{-4}. The reflected laser beam is detected by a photodiode, the output of which is processed through a phase sensitive amplifier and read into a computer. Also, the radiation that is scattered by the front and back interfaces of the growing film into a solid angle of 5° is focused by a lens at a location well removed from the plane of incidence of the impinging light beam onto the entrance
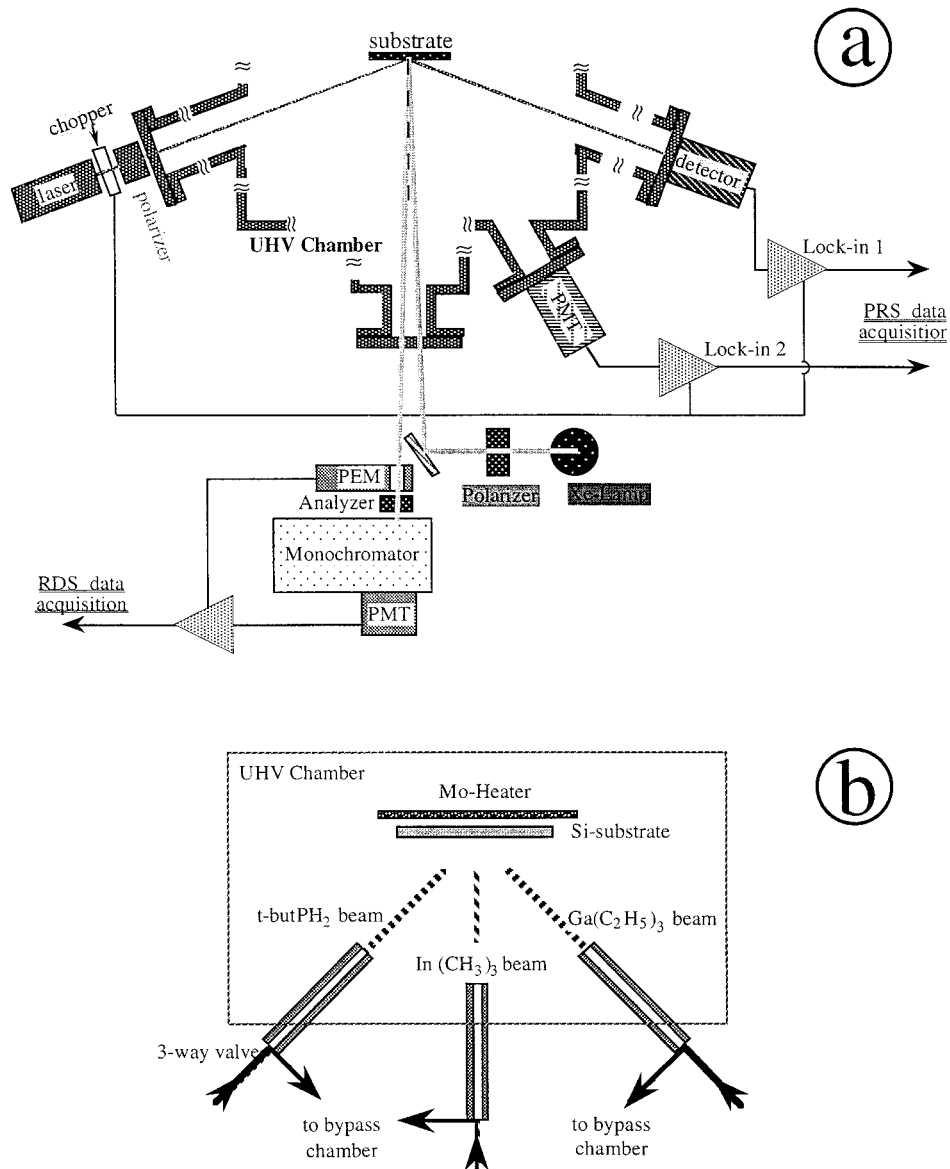

FIG. 1. Schematic representation of (a) the vacuum chamber with real-time optical process monitoring ports for single-wavelength PR, LLS, and RDS. (b) Schematic representation of source vapor switching and substrate stage.

slit of a photomultiplier. Because of its technological significance, most of the experimental data discussed here refer to the Si(100) substrate surface, including vicinal surface orientations, misoriented toward [011]. Upon appropriate surface conditioning, the misorientation for such vicinal surfaces is accommodated by double steps parallel to the [0$\bar{1}$1] direction, which are energetically favored with regard to single steps and result in large (2×1) domains with parallel dimer rows on the top and bottom surfaces of the step.[5]

The single-wavelength PR intensity shows periodic variations in time due to interference between the partial waves reflected at the top and bottom interfaces of the heteroepitaxial GaP as illustrated in Fig. 2(a). The periodicity of these oscillations is related by analytic expressions to the thickness of the growing epilayer and can be utilized to calculate the growth rate in real time, which is reviewed in detail in Ref.

3. Superimposed to the interference oscillations is a fine structure that varies periodically with the periodicity of the source vapor pulse sequence. Figure 2(a) shows the PR intensity as a function of time over a period of growth corresponding to several interference fringes, and in the inset the magnified fine structure in the region of the second maximum. In the particular experiment of Fig. 2 the LLS intensity exhibits only weak variations, that is, the surface roughness does not undergo a large change from start to finish of the experiment. The top part of Fig. 2(b) shows a schematic representation of the pulse sequence, consisting of a t-butPH$_2$ pulse that is followed by pause No. 1, a TEG pulse followed pause No. 2 and so on. The bottom part of Fig. 2(b) shows the associated response in the PR intensity. From the periods in the interference fringes and the precursor cycle the average incremental increase of the GaP epilayer thickness
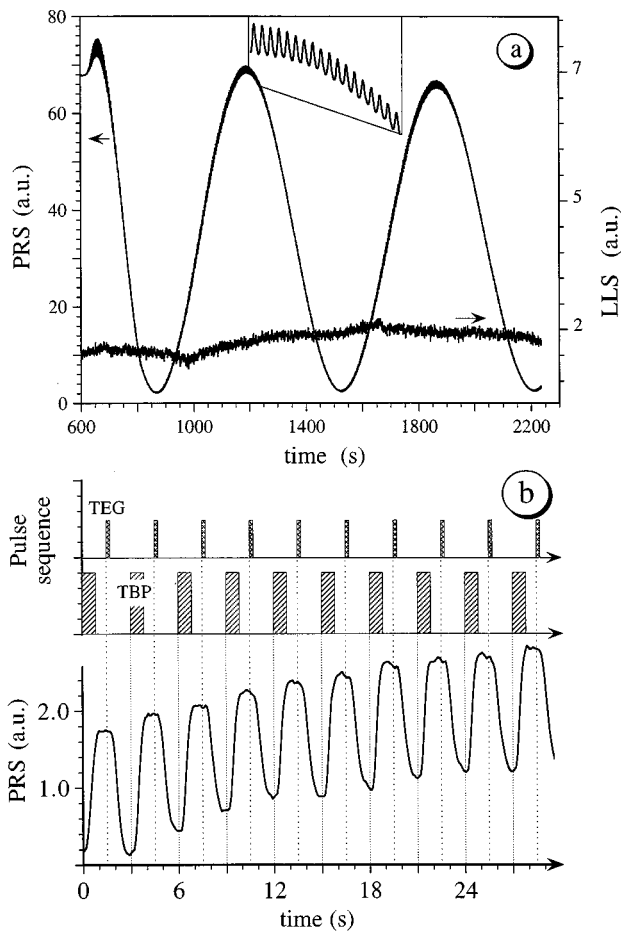
FIG. 2. (a) PR intensity as a function of time for pulsed CBE growth of GaP on Si(100), (b) pulse sequence and the associated PR fine structure.

FIG. 3. Cross sectional HREM image of a GaP/Si(100) interface prepared by CBE using TEG and TBP as source materials.

per cycle can be determined for steady state growth with an accuracy of approximately 5%. The measured time-dependent LLS intensity provides information on the roughness of the top and bottom interfaces of the film.

III. CONTROL OF DEFECT FORMATION/PROPAGATION

At room temperature, GaP has a lattice constant of 5.4512 Å that nearly matches the lattice constant of Si of 5.4301 Å. Exact lattice matching of the III–V epilayer to the silicon substrate is possible at a chosen temperature through alloying, e.g., formation of a GaN_yP_{1-y} solid solution of the appropriate composition.[6] However, the difference in the thermal expansion coefficients for the epilayer and the substrate invariably results in the generation of strain upon thermal cycles in the processing. Also, antiphase domains (APDs) are formed irrespective of misfit strain upon III–V heteroepitaxy on group IV substrate surfaces that exhibit single steps or odd multiples thereof.[7] Fortunately, one APD variant often outgrows the other, so that the APDs remain restricted to regions close to the heterointerface.[8]

At interfaces between singular Si and III–V faces that are polar, such as {100} or {111}, either faceting into nonpolar

surface elements, such as {110} or {112}, or intermixing have been predicted based on assessments of interface charge.[9] Figure 3 shows a high resolution transmission electron microscopy (HREM) image of a cross section of a GaP/Si(100) heterostructure created by pulsed CBE. No evidence for faceting is observed. However, charge build-up at the polar interface can contribute to interface broadening. In addition, there are other mechanisms of interface broadening such as interdiffusion, which may be enhanced by the formation of native point defects as part of the interfacial reactions. Therefore, it is presently impossible to determine whether or not electrostatic effects play a significant role. Recent STM investigations provide insights into the early stages of the interactions of the Si(100) 2×1 surface with phosphine.[10,11] At low to intermediate dose, the Si dimers on the Si(100) 2×1 surface are completely replaced by Si–P heterodimers, pushing Si surface atoms from their original Si-dimer positions into adatom positions. Since these Si adatoms are likely to become incorporated into the epitaxial film upon further growth, they contribute to interface broadening. On the P-saturated surface, the Si–Si dimers are replaced by P–P homodimers generating surface strain that is relieved, in part, by the generation of shallow trenches parallel to the dimer rows that are bound by elongated {111} facets and can affect the kinetics of subsequent heteroepitaxial overgrowth.[12] In particular, the {111} facets in the Si(100) surface upon overgrowth by GaP can act as nucleation sites for the formation of stacking faults that propagate deeply into the heteroepi-
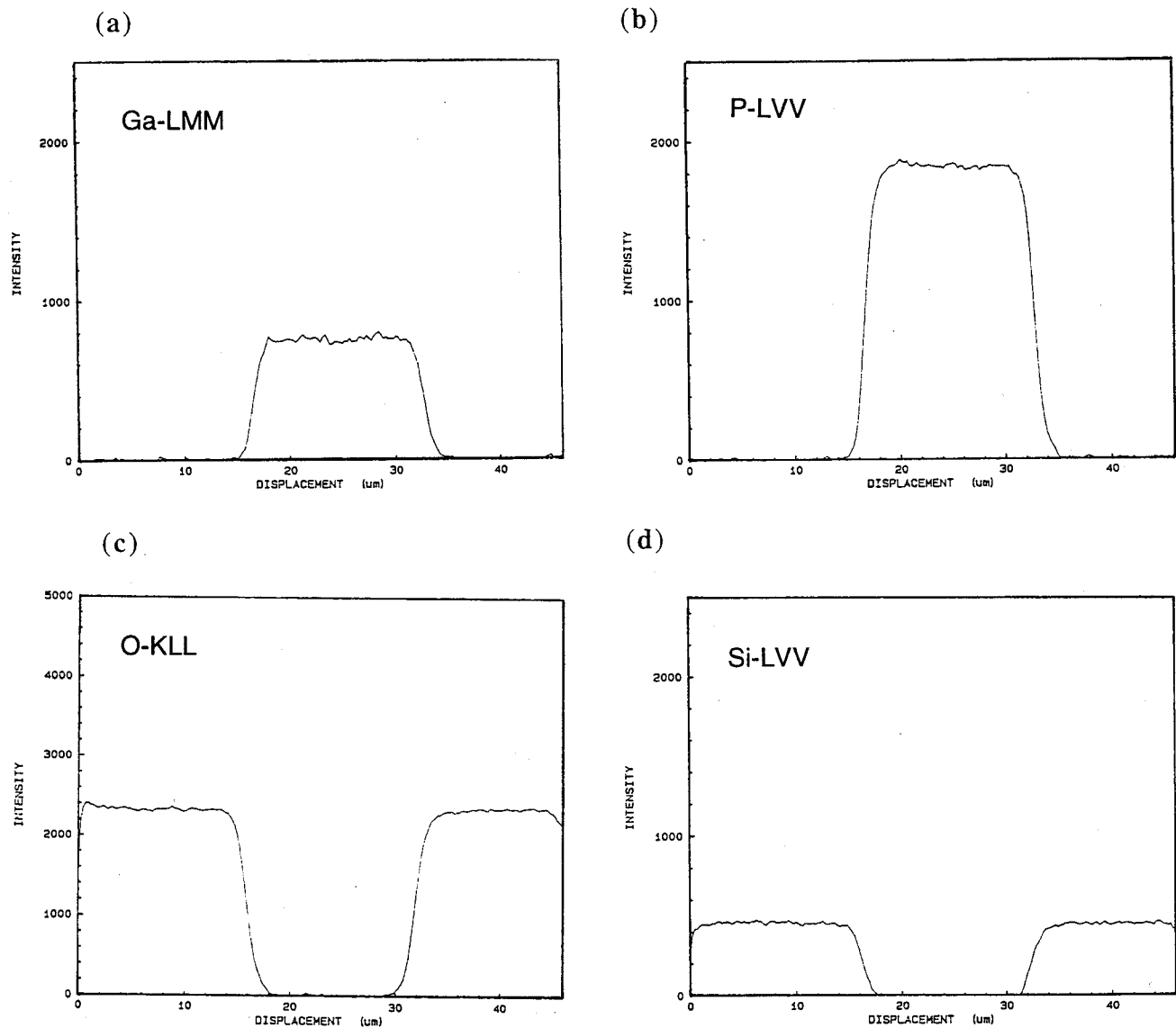
FIG. 4. Auger electron spectroscopy line scans at the energies of the (a) Ga-LMM, (b) P-LVV, (c) O-KLL, and (d) Si-LVV lines over a SiO_2-masked silicon surface with 10×10 μm window areas filled with epitaxial GaP.

taxial film. Driving the phosphorus coverage of the surface to saturation thus is not necessarily a desirable condition of GaP heteroepitaxy on Si, which must be weighed against the control of stoichiometry, requiring large V:III source vapor flux ratio.

An important cause of defect formation is residual contamination of the silicon surface. In our experiments, a modified RCA cleaning procedure ending with an aqueous HF dip was used to create a hydrogen-passivated Si(100) 1×1 surface prior to transfer into the CBE chamber through a load-lock. This initial reconstruction was verified by RHEED. The control of the pH and the concentration of the etching solution, absence of dissolved oxygen, and the conditions of oxidation prior to HF (or, for {111} substrate wafers, NH_4F) etching are all important factors in controlling the surface roughness and chemical integrity of the hydrogen-terminated silicon surface.[13–15] Recent quantitative high resolution XPS

studies of carefully prepared hydrogen-terminated Si(001) (1×1) surfaces revealed surface concentrations of residual oxygen and fluorine atoms in the mid-10^{12} cm^{-2} range.[16] Because of the high selectivity of the epitaxial growth of GaP on Si vs SiO_2, this level of residual contamination can make a significant contribution to the generation of defects.

Figure 4 shows Auger electron spectroscopy (AES) line scans across 10×10 μm windows in a SiO_2 mask on a Si(100) substrate after deposition of heteroepitaxial GaP in the window areas at (a) 120, (b) 1070, (c) 510, and (d) 92 eV. They reveal a substantially larger kinetic barrier to nucleation of GaP on the SiO_2-masked surface areas as compared to the bare Si window areas. Although high selectivity is a welcome property in the context of device fabrication, in the context of defect formation, the kinetic barrier to overgrowth of surface areas contaminated by oxygen is a detriment. Upon forced overgrowth of such contaminated surface

patches, defects may form in the epitaxial film due to the generation of strain. This strain may be relieved by the formation of 60° dislocations that dissociate into partials. Also, for amorphous contaminant patches, loss of registry to the underlying substrate lattice can cause the formation of stacking faults. Similar experiments conducted on partially SiC-coated Si surfaces show that the overgrowth by GaP is also highly selective with regard to SiC, that is, carbon contamination of the silicon surface is also of concern. Burying the surface contaminants under a homoepitaxial layer of silicon that exposes a virgin surface at the initiation of heteroepitaxy can result in improvements, because the stacking fault energy for silicon (65 mJ/m^2) is substantially larger than for GaP (41 mJ/m^2).[17] The relatively small stacking fault energy of GaP is a consequence of the decrease of the stacking fault energy in the zincblende structure III–V compounds with increasing ionicity of the bonding. Thus, the structure becomes unstable in the electronegativity difference range between AlP, which has zincblende structure at slightly larger lattice constant than silicon and InN that has wurzite structure at smaller lattice constant than silicon. Therefore, the insistence on nearly lattice-matched materials combination generates conditions, where the gains in minimizing strain are paid for by losses in maximizing the probability of stacking errors. Indeed, high densities of stacking faults have been observed in GaP/Si(100) heterostructures by TEM.[18]

Since in zincblende structure compounds stacking faults nucleate on {111} and, for GaP growth on Si(100), the GaP nuclei are bound by {111} facets,[18] the formation of three-dimensional faceted GaP islands in the initial period of nucleation and overgrowth of the Si surface must be curtailed to control the density of planar defects in the heterostructure. The aspect ratio A of height to width of the nuclei depends on both thermodynamic and kinetic parameters. The assessment of habit of heteroepitaxial nuclei governed by thermodynamics is possible on the basis of the modified Wulff's law

$$\frac{\sigma_{hkl} - \alpha_{hkl}}{r_{hkl}} = \frac{\Delta\mu}{2v}, \tag{1}$$

stating that the habit of the nuclei—formed under the conditions of heteroepitaxy on the substrate surface of orientation (hkl)—is related to the equilibrium habit of homogeneously formed three-dimensional nuclei at same supersaturation $\Delta\mu$ by truncation.[19] This truncation is characterized by central distance r_{hkl} in the heterogeneously formed nucleus to the interface of orientation (hkl), which, for a given supersaturation and volume v of the crystal building blocks, depends on the relative magnitudes of surface free energy σ_{hkl} on the facet (hkl) on the homogeneously formed nucleus and the interfacial attachment energy α_{hkl}. A three-dimensional nucleation mechanism thus ensues for $0 < \alpha_{hkl} < 2\sigma_{hkl}$, with decreasing aspect ratio A (height/width) of the three-dimensional nuclei for increasing α_{hkl}, approaching a two-dimensional nucleation and growth mechanism in the limit $\alpha_{hkl} \rightarrow 2\sigma_{hkl}$. However, in addition to thermodynamic causes for three-dimensional overgrowth, kinetic enhancements of

A results from the catalysis of TBP decomposition on the GaP surface elements.[20] Upon growth, the three-dimensional nuclei thus formed expand laterally and meet with patches of surface contaminants that are randomly distributed on the silicon surface. In view of the large barrier to GaP growth on the surface of the oxide patch, its overgrowth by the GaP nucleus requires a substantial fluctuation in the chemical potential that, given the relatively low stacking fault energy, results in a high probability of stacking fault formation. Although it is thus difficult to avoid the nucleation of stacking faults, their propagation into the III–V epilayer can be minimized by structuring of the Si(100) surface into V groves bound by (111) and ($\bar{1}11$) facets along [$0\bar{1}1$]. This concept has been applied successfully in controlling stacking fault propagation in InP/Si(100) heterostructures.[21–24]

The blockage of the propagation of stacking faults is explained by interactions between the partial dislocations that support them. Stacking faults form upon dissociation of unit 60° dislocations on (111) and ($\bar{1}11$) according to

$$\mathbf{b}_1 = \frac{a}{2}[\bar{1}10] = \frac{a}{6}[\bar{2}11] + \frac{a}{6}[\bar{1}2\bar{1}] = \mathbf{b}_2 + \mathbf{b}_3, \tag{2}$$

$$\mathbf{b}_4 = \frac{a}{2}[101] = \frac{a}{6}[211] + \frac{a}{6}[1\bar{1}2] = \mathbf{b}_5 + \mathbf{b}_6, \tag{3}$$

respectively, where $\mathbf{b}_1$ and $\mathbf{b}_4$ refer to the Burgers' vectors of the 60° dislocations and $\mathbf{b}_2$, $\mathbf{b}_3$ and $\mathbf{b}_5$, $\mathbf{b}_6$ refer to the Burgers' vectors of the associated partials. This is illustrated in Fig. 5(a). Because of their smaller length as compared to $\mathbf{b}_1$ and $\mathbf{b}_4$, the dissociation reactions are energetically favored and provide a driving force for the generation of the stacking faults suspended between the partials. For InP, which has a stacking fault energy of 18 mJ/m^2, large separations between the partials have been observed.[25] Therefore, for submicrometer groove depth, the faults can expand after nucleation over the entire V-groove facet. Upon interaction between the partials with Burgers' vectors $\mathbf{b}_3$ and $\mathbf{b}_6$ on the intersection of the two glide planes according to

$$\frac{a}{6}[1\bar{1}2] + \frac{a}{6}[\bar{1}2\bar{1}] \rightarrow \frac{a}{6}[011] = \mathbf{b}_7, \tag{4}$$

Lomer–Cottrell sessile dislocations of pure edge character can be formed. Although this dislocation cannot move by glide, in principle, it can move by climb. However, dislocation climb in this case is tagged to motion of the entire stacking fault, which is highly unlikely. In view of the polar nature of the dislocations and possible presence of other defects, that is, APBs and misfit dislocations near the interface, more complex interactions can occur and require further study. Also, the above discussed mechanism of self-termination of stacking fault propagation relies on perfect faceting at a submicrometer scale and the absence of nucleation of stacking faults on {111} variants other than (111) and
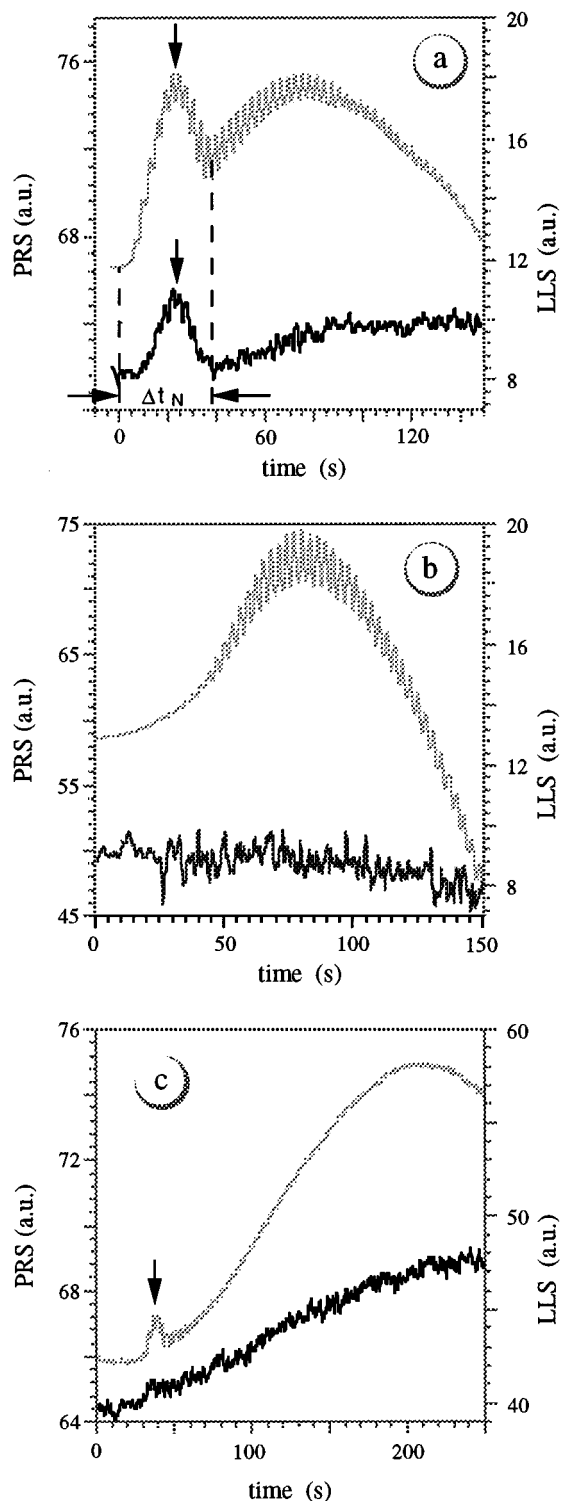
FIG. 5. Initial PR intensity traces for pulsed CBE of GaP on Si(100): (a) at small Ga supersaturation; (b) under optimized processing conditions; (c) at large Ga supersaturation.

($\bar{1}$11) due to the faceting of three-dimensional GaP nuclei or uncontrolled formation of microfacets. The first of these two potential problems can be addressed on the basis of optical process monitoring during the initial phase of GaP nucleation and overgrowth of the Si surface by a contiguous GaP film.

IV. INITIAL PHASE OF NUCLEATION AND OVERGROWTH

Since, under the conditions of vapor phase epitaxy, the dielectric function of the ambient is smaller than the dielectric function of the deposited compound, a corrugated incomplete heteroepitaxial film is associated with an effective dielectric function that increases with decreasing pore size upon progressive overgrowth of the substrate surface from initially close to the ambient dielectric function to the dielectric function of the contiguous heteroepitaxial film. Consequently, during this initial phase of heteroepitaxy, distinct features are observed in the time-dependent PR intensity, marked by a vertical arrow in Fig. 5(a). Figures 5(a)–5(c) represent a set of experiments carried out under the same conditions, except for different TEG flux in the initial 20 s of the experiment. At small TEG flux, that is, small supersaturation of the surface with regard to Ga precursors to growth, the low nucleation rate results in the formation of widely spaced nuclei that grow to substantial height before coalescing into a contiguous epilayer. The associated roughening of the surface is observed in Fig. 5(a) in the time-dependent LLS intensity and is also marked by a vertical arrow. At the time of complete coverage of the substrate surface by a contiguous heteroepitaxial film, that is, at the end of the period labeled Δt_N, the reflectance and LLS signals merge into the time dependence for contiguous film growth. The magnitude of the PR and LLS intensity changes in this initial period Δt_N depends on the aspect ration A of the height to width of the GaP islands. *Ex situ* atomic force microscopy investigations reported by us elsewhere confirm the roughening of the surface relative to the initial roughness of the silicon surface in the nucleation period under the conditions of Fig. 5(a), the subsequent smoothening of the epilayer, once a contiguous GaP film has been formed, and the increase of surface roughness upon further growth.[26] This correlation of the initial feature during the nucleation stage to significant roughening in the later stages of steady-state film growth has been observed consistently in several experiments. Therefore, we conclude that improvements in the control of A in the initial nucleation and overgrowth phase can affect the quality of the epilayer during later stages of growth.

Figure 5(b) shows the result of increasing the TEG flux in the first 20 s of the nucleation and overgrowth period at the same TBP flux as in Fig. 5(a), increasing the supersaturation on the surface. Since at higher supersaturation a higher density of nuclei of smaller height is generated and an increased supply of nutrients exists between these islands, they merge into a contiguous film upon a shorter period of lateral growth. In addition, the higher Ga supersaturation on the silicon surface elements between the GaP nuclei should reduce the local differences in the catalytic properties on the partially GaP coated surface. In contrast to Fig. 5(a), no excess intensity in the time-dependent PR and LLS signals is observed during the initial phase of film formation under the conditions of Fig. 5(b). However, there exists a sensitive upper limit in the initial increase of the TEG flux at a given TBP flux, above which gallium droplets form. Also, the tim-

ing of the merging of the initially higher TEG flux into the smaller optimum TEG flux for steady-state growth of the contiguous heteroepitaxial film is critical to avoid phase separation on the surface. Thus, upon exceeding a critical upper limit for the gallium supersaturation, surface roughening due to Ga droplet formation results in a rapid deterioration of the surface morphology, as illustrated in Fig. 5(c), which shows a clearly resolved nucleation peak in the PR intensity—marked by a vertical arrow—and an immediate continuous rise in the LLS intensity that accelerates in later periods of growth not shown in Fig. 5(c). Under extreme conditions, a vapor–liquid–solid (VLS) growth mechanism may take over, leading to very large aspect ratios of the surface features.

V. KINETICS OF STEADY-STATE HETEROEPITAXIAL GROWTH

Details of the growth kinetics after complete sealing of the silicon surface by a contiguous GaP film are revealed by the response in the time-dependent PR intensity to variations in the source vapor cycle and perturbations of the steady-state surface composition. For example, in a preceding publication,[27] we have shown that the growth rate per cycle v_c for constant source vapor pulse heights and widths is insensitive to the duration of pause No. 1 between the trailing edge of the TBP pulse and the leading edge of the following TEG pulse. However, v_c increases with increasing length of pause No. 2 between the trailing edge of the TEG pulse and the leading edge of the following TBP pulse. We interpreted this result as a consequence of a kinetic barrier to the complete dealkylation of the impinging TEG molecules on the GaP surface. Their conversion into surface species that contribute to the growth, for example, Ga surface atoms, represents the time limiting step in the heteroepitaxial growth process. Thus, a reservoir of TEG fragments that do not directly contribute to epitaxial growth coexists on the surface with active fragments that are derived from the inactive fragments over time and feed the GaP growth. Since v_c can correspond to several bilayers of GaP per cycle,[6] in steady state, a store of up to several monolayers of the source vapor fragments must exist on the surface to sustain the growth. Therefore, the modeling of steady-state heteroepitaxial growth must be based on a four-layer stack: (a) ambient; (b) surface reaction layer (SRL); (c) heteroepitaxial film; (d) substrate. The SRL is strictly stabilized by the kinetics of the primary pyrolysis and follow-up reactions. Since only part of the molecules in the SRL are attached to the surface, under this specific condition of pulsed CBE, part of the chemical reactions on the surface proceed homogeneously between molecules that not at all or only weakly bound to the surface atoms of the GaP film and consequently are randomly oriented. Thus, a set of coupled parallel and consecutive homogeneous reactions within the SRL proceed simultaneously with heterogeneous surface reactions and crystallization processes. The latter heterogeneous reactions are coupled to the homogeneous reactions through intermediates. However, there exist also competing reaction pathways, e.g., β elimination of radical ligands by reaction with adsorbed hydrogen atoms in parallel to homogeneous radical chemistry in the SRL. Since the bonding of products to the surface strengthens as the radical ligands are shed, the homogeneous reactions will dominate the initial steps of dealkylation while denuded products, such as Ga and P atoms that bond strongly to the surface and eventually incorporate into the GaP lattice, will probably not be present at large concentration in the random part of the SRL.

The complex reflectivity coefficient for p-polarized light impinging onto the four-layer stack for a specific value of the film thickness can be calculated on the basis of the Fresnel equations.[28] In addition to knowledge of the dielectric functions of the Si substrate, the GaP film, and the ambient, the angle of incidence and wavelength this requires an assessment of the dielectric function of the surface reaction layer and its thickness. Generally, both the dielectric function and thickness of the SRL are functions of time.

For a preliminary assessment, we recently introduced a simplified model that reduces the complex surface reaction scheme discussed above to an exponential build up of t_b upon exposure of the surface to a pulse of TBP, followed by an exponential decay to zero thickness after supply of the pulse of TEG, which is accompanied by an incremental increase in the thickness of the GaP epilayer.[29] This model reveals two important features in the PR intensity:

(i) A periodic increase and decrease in the amplitude of the fine structure that is tagged to the interference oscillations. The relative positions of minima in the fine structure amplitude with respect to the positions in the minima of the interference oscillations depend on the value of the dielectric function of the SRL.

(ii) A change of the signs of the response to the TBP and TEG pulses at the minima in the fine structure amplitude. Because of the turnover in the pulse response at these positions, we refer to them as turning points in the PR fine structure.

Here we expand the model by adding an assessments of the changes in the dielectric function due to changes in the composition of the homogeneous part of the SRL as the growth process progresses. Since in this case the molecules are randomly spaced and oriented the electronic transitions, contributing to the dielectric function refer to localized states. Thus, the dielectric function can be represented by a modification of the Sellmeier equation, summing the contributions of all constituent molecules, that is,

$$\epsilon_b = 1 - \frac{4\pi}{V} \sum_l \sum_k \sum_{Q'_{kl}Q_{kl}} \frac{2|\xi\mu'_{QklQkl}|^2 E'_{QklQkl}}{E_+^2 - E'^2_{QklQkl}}, \quad (5)$$

where V is the volume of the surface reaction layer, ξ and μ'_{QklQkl} represent the unit polarization vector and the matrix element of the electric dipole operator for the electronic transition between filled states Q_{kl} and empty states Q'_{kl} associated with the individual molecule labeled by subscript k of the constituent labeled by subscript l, E'_{QklQkl} is the energy of this transition, and $E_+ = \hbar\omega_+ = \hbar(\omega + i\eta)$ is the energy at which ϵ_b is evaluated in the limit of turn-on parameter

$\eta \to 0^+$. Since all molecules of a particular constituent have same molecular orbitals and electric dipole-allowed transitions, the summation over k results simply the number of molecules of each species. Also, the number of molecules of one particular constituent l—divided by the volume—represents its concentration c_1 in the surface reaction layer. Therefore, Eq. (5) provides for the desired correlation between the composition of the homogeneous part of the SRL and the dielectric function.

However, Eq. (5) does not account for intermolecular interactions, which in view of the high concentrations of at least some of the constituents must be considered. Therefore, we replace the concentrations of all constituents of the surface reaction layer by activities, that is, $a_1 = f_1 c_1$, with a specific activity coefficient $f_1 \neq 1$ for each constituent that generally depends on both temperature and composition. Then,

$$\epsilon_b = 1 - 4\pi \sum_l a_l \sum_{Q'_l Q_l} \frac{2|\xi \mu'_{QlQl}|^2 E'_{QlQl}}{E_+^2 - E'^2_{QlQl}}, \tag{6}$$
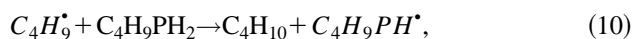
where the first sum extends over all constituents of the surface reaction layer and the second sum extends over the electric dipole allowed transitions from filled states for each of these constituent molecules.

Note that Eqs. (5) and (6) rely on the assumption that the volume of the surface reaction layer is constant in time, which holds only in the limit of small variations in its composition. Therefore, we restrict in the following discussion of specific correlations between surface reaction layer composition and responses in the PRS intensity to experiments carried out at constant temperature with a preceding reproducible surface conditioning step and small variations in composition. Within these restrictions, the activity coefficients can be considered to be constants, which enables the analysis of the homogeneous reactions in the SRL on the basis of analytic expressions for the integrated rate laws.
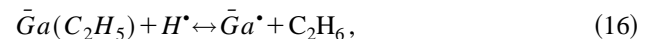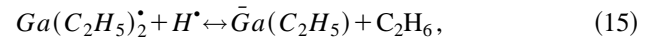
The pyrolysis of the primary source molecules impinging onto the SRL is represented by

$$C_4H_9\bar{P}H_2 \to C_4H_9^\bullet + \bar{P}H_2^\bullet, \tag{7}$$

$$Ga(C_2H_5)_3 \to Ga(C_2H_5)_2^\bullet + C_2H_5^\bullet. \tag{8}$$
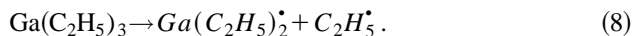
In these equations, fragments located in the SRL are represented in italics and molecules that are expelled into the vapor phase and pumped off are represented in plain lettering. The *t*-butyl-phosphine fragments and ethyl radicals can decompose further under the generation of adsorbed hydrogen atoms according to

$$C_2H_5^\bullet \to C_2H_4 + H^\bullet, \tag{9}$$

$$C_4H_9^\bullet + C_4H_9PH_2 \to C_4H_{10} + C_4H_9PH^\bullet, \tag{10}$$

$$C_4H_9PH^\bullet \to C_4H_9 + |\bar{P}H, \tag{11}$$

$$C_4H_9^\bullet \to C_4H_8 + H^\bullet, \tag{12}$$

$$\bar{P}H_2^\bullet \to |\bar{P}H + H^\bullet, \tag{13}$$

$$|\bar{P}H \to |\bar{P}^\bullet + H^\bullet, \tag{14}$$

that assist the dealkylation of the TEG fragments on the surface according to

$$Ga(C_2H_5)_2^\bullet + H^\bullet \leftrightarrow \bar{G}a(C_2H_5) + C_2H_6, \tag{15}$$

$$\bar{G}a(C_2H_5) + H^\bullet \leftrightarrow \bar{G}a^\bullet + C_2H_6, \tag{16}$$

in competition with

$$C_2H_5^\bullet + H^\bullet \to C_2H_6, \tag{17}$$

$$C_4H_9^\bullet + H^\bullet \to C_4H_{10}, \tag{18}$$

$$|\bar{P}H + H^\bullet \to \bar{P}H_2^\bullet, \tag{19}$$

$$\bar{P}H_2^\bullet + H^\bullet \to \bar{P}H_3, \tag{20}$$

and

$$H^\bullet + H^\bullet \to H_2. \tag{21}$$

The final step in the overall reaction of TBP and TEG to form GaP is the incorporation of Ga and P atoms into the GaP lattice. As established in a series of experiments using deuterated TBP by Li *et al.*[30] for the growth of GaP using TBP and trimethylgallium (TMG) as source vapors, adsorbed PH_2 and PH radicals play an important direct role in the pyrolysis of both TBP according to reactions (11)–(14) and TMG according to

$$PH_x + Ga(CH_3)_y \to PH_{x-1} + Ga(CH_3)_{y-1} + CH_4,$$

$$x = 1,2 \quad \text{and} \quad y = 1,2. \tag{22}$$
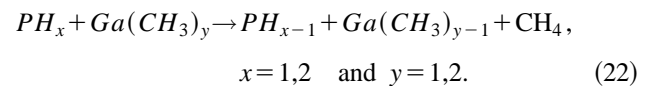
Although there exist significant differences in the interactions of TEG and TMG fragments with the GaP surface, we expect that adsorbed PH_x also plays an important role in the heterogeneous dealkylation of TEG and its fragments. All reactants and products shown in the equations in italics contribute to the composition of the surface reaction layer, which exists strictly on the basis of kinetic barriers to the desorption of its constituents, with the exception of gallium, which has at the growth temperature a vapor pressure well below the background pressure in the reactor. We note that the set of equations written above is not exhaustive; that is, other reactions may be added as our knowledge of details grows. Since the heterogeneous reactions that contribute to crystal growth probably entail competition for active surface sites and replacement of inhibitors at such sites, it is reasonable to expect that they will be slower than the homogeneous radical reactions in the SRL. Also, the denuded fragments, e.g., gallium atoms and possibly monoethyl gallium (MEG), are expected to be bonded tighter to the surface than organometallic fragments that retain several ligands, e.g., diethylgallium (DEG). Therefore, we limit the discussion of the homogeneous kinetics onto reactions involving primary and secondary products of the pyrolysis reaction. Under conditions of pulsed growth, the concentrations and activity coefficients of all reactants and products vary with time, and reactions (9)–(22) are coupled through the bimolecular reactions, having surface hydrogen as one of the reactants. No
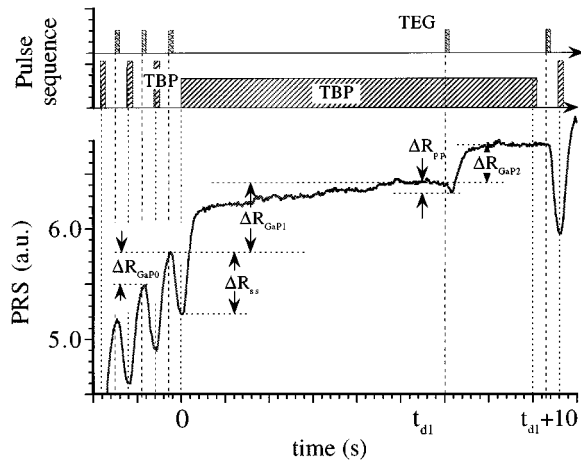
FIG. 6. Schematic representation of the timing of the source gas flow (top) and response in the PR intensity to a TEG probe pulse during interruptions of steady state and switching to continuous TBP flow (0.8 sccm) during the interruption.
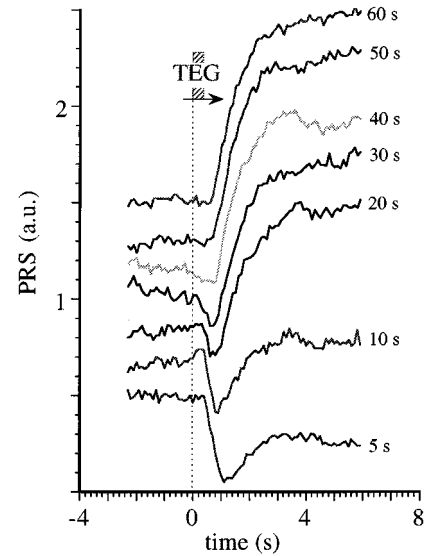

FIG. 7. Single wavelength PRS response to the TEG probe pulse under the conditions of Fig. 9 at $\lambda = 632.8$ nm for selected values of t_{d1}.

analytical solutions are available for the quantitative analysis of the PR intensity, in this case requiring the application of numerical methods.

Considerable simplifications are gained under the conditions of interrupted steady-state growth, where the TEG pulses are switched off at initiation time t_{int}, continuing the exposure of the surface to a continuous TBP flux, as illustrated in Fig. 6. Since we use in our experiments typically TBP to TEG flux ratios in the range 10:1 to 40:1, at constant TBP flux, the hydrogen and phosphorus activities in the SRL are only marginally perturbed by the TEG probe pulse and can be taken as constants during the delay period t_{d1}. Going back to Fig. 5(b), we note that initially the PR response to the application of TEG pulses after heating the surface of the substrate under TBP exposure to the growth temperature is very small. The development of the fine structure to full swing from low PR intensity after application of the TEG pulse to high PR intensity after the TBP pulse requires several cycles. Also, we note that in Fig. 6, the response in the PR intensity ΔR_{pp} to a TEG probe pulse at a delay t_{d1}, after switching from pulsed to continuous TBP flow and discontinuation of TEG pulse supply at time t_{int}, is substantially smaller than the response to the last TEG pulse under steady-state conditions ΔR_{ss}. We interpret these features in Figs. 5(b) and 6 as being due to the build-up of the surface reaction layer under the conditions of initial nucleation and overgrowth and its destruction upon interruption of steady-state growth, respectively, that is, relate ΔR_{pp} to the deviations of the surface reaction layer from steady state, which includes its coupling to the surface of the substrate. Thus, we can utilize the response to a TEG probe pulse for an assessment of the kinetics of the chemical changes in the reaction layer upon perturbations of steady state, e.g., switching from pulsed to continuous TBP flow and discontinuation of TEG pulse supply.

In the following discussion, we set $t_{int} \equiv 0$, that is, measure t_{d1} from $t = 0$ to the rising edge of the TEG probe pulse. The

exposure to the continuous TBP beam is maintained for a period $t_{d1} \leq t \leq t_{d1} + t_r$. The time interval t_r refers to the recovery period after the application of the TEG probe pulse in the PR intensity before reconditioning the surface to steady-state growth for the next experiment and is typically 10 s. A considerable number of experiments can be conducted within one heteroepitaxial growth run. Comparisons between experiments from several runs were made to establish the reproducibility of our findings. All experiments described below applied the same pulse cycle sequence for conditioning to steady-state growth. Figure 7 shows the decrease in the amplitude of the response in the PR intensity to the TEG prove pulse fort selected values of t_{d1} of increasing in length. Note that, in view of the increase in the amplitude of the PR intensity with increasing distance from the turning points, the response to the TEG probe pulse in a particular experiment depends on the timing of the experiment relative to the extrema in the interference oscillations. In the following evaluations, this effect is eliminated by normalization of ΔR_{pp} to ΔR_{ss}.

Figures 8(a) and 8(b) show plots of the normalized measured response $\Delta R_N \equiv \Delta R_{pp}/\Delta R_{ss}$ versus t_{d1} for two experiments under the conditions of Fig. 6. The curves labeled exp represents cubic spline fits to the experimental data. While for a given set of experimental parameters, the initial decrease of ΔR_N with time is reproducible, after 5–10 s, variations between different experiments are observed. This is interpreted in terms of the kinetics of the chemical reactions on the GaP surface, starting with the decay of DEG radicals according to Eq. (15). The rate law for this reaction step is of the form

$$-\frac{da_{Ga(C_2H_5)_2}}{dt} = k_{15} a_H a_{Ga(C_2H_5)_2}.$$ (23)

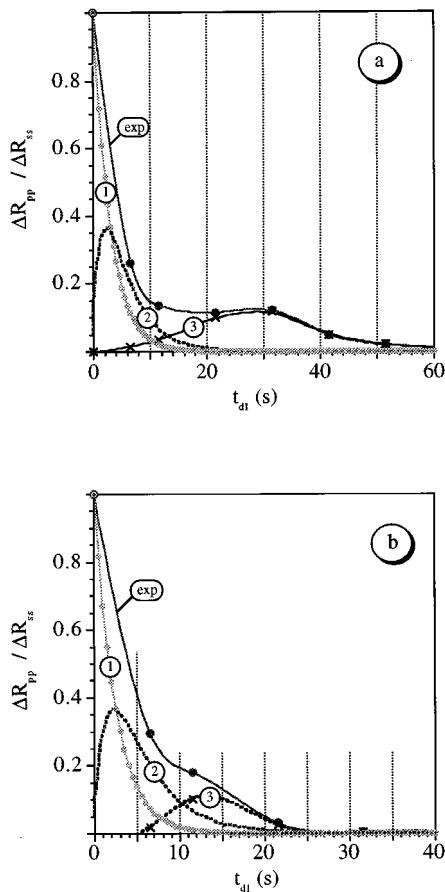Since at large constant flux of TBP, the activity of hydrogen

FIG. 8. Plot of $\Delta R_{pp}/\Delta R_{ss}$ vs time delay t_{d1}—measured from last TEG pulse under steady-state conditions of growth—to the application of a single TEG probe pulse: curve 1 based on Eqs. (6) and (25), curve 2 based on Eqs. (6) and (28). (a) and (b) refer to two different experiments run under the same conditions.

in the surface reaction layer a_H at $t \geq 0$ is only slightly perturbed by the ongoing surface reactions, we may in a first approximation treat it as a constant, that is, rewrite Eq. (23) as

$$-\frac{da_{Ga(C_2H_5)_2}}{dt} = k'_{15} a_{Ga(C_2H_5)_2}. \tag{24}$$

With initial condition $a_{Ga(C_2H_5)_2}(t=0) = \bar{a}_{Ga(C_2H_5)_2}$, we thus get the integrated rate law

$$a_{Ga(C_2H_5)_2}(t) = \bar{a}_{Ga(C_2H_5)_2} \exp\{-k'_{15}t\}$$

$$\approx \bar{a}_{Ga(C_2H_5)_2} \exp\left(-\frac{t}{\tau_1}\right), \tag{25}$$

that is, the DEG activity decays from the value established in steady state $\bar{a}_{Ga(C_2H_5)_2}$ at $t=0$ exponentially with time constant $\tau_1 = 1/k'_{15}$, that is, $k'_{15} = 0.4 \text{ s}^{-1}$. We note that under the conditions of the experiment the activities of PH_x are also constants, so that adding Eq. (22) as a parallel reaction path merely changes the interpretation of k'_{15}, but not the rate equation.

The time evolution of the activity of monoethylgallium (MEG) in the surface reaction layer is composed of a contribution to the MEG activity $\Delta a_{Ga(C_2H_5)}$—generated in the course of the decay of the DEG according to reaction (15)—that adds at $t>0$ to the activity of MEG $\bar{a}_{Ga(C_2H_5)}$ measured at $t=0$. By reaction (15), the rate with which this contribution is generated is coupled to the rate of the DEG decay according to

$$\frac{d(\Delta_{Ga(C_2H_5)})}{dt} = -\frac{d(a_{Ga(C_2H_5)_2})}{dt}. \tag{26}$$

Also, with the assumption of constant hydrogen activity, the rate law for reaction (16) can be written as

$$-\frac{da_{Ga(C_2H_5)}}{dt} = k_{r16} a_H a_{Ga(C_2H_5)} = k'_{16} a_{Ga(C_2H_5)}. \tag{27}$$

Therefore, we get

$$a_{Ga(C_2H_5)}(t) = \left[\bar{a}_{Ga(C_2H_5)} + k'_{15} \bar{a}_{Ga(C_2H_5)_2} \right.$$

$$\times \left. \int_0^t \exp\left(-\frac{t}{\tau_1}\right) dt \right] \exp(-k'_{16}t)$$

$$= \left\{ \bar{a}_{Ga(C_2H_5)} + \bar{a}_{Ga(C_2H_5)_2} \left[1 - \exp\left(-\frac{t}{\tau_1}\right) \right] \right\}$$

$$\times \exp\left(-\frac{t}{\tau_2}\right), \tag{28}$$

where $\tau_2 = 1/k'_{16}$. This function has a single extremum at

$$t_{max} = \tau_1 \ln\left(\frac{\bar{a}_{Ga(C_2H_5)_2}}{\bar{a}_{Ga(C_2H_5)2} + \bar{a}_{Ga(C_2H_5)_2}} \frac{\tau_1 + \tau_2}{\tau_1} \right) \geq 0 \tag{29}$$

and initial slope

$$\frac{da_{Ga(C_2H_5)}}{dt}\bigg|_{t=0} = \frac{\bar{a}_{Ga(C_2H_5)_2}}{\tau_1} - \frac{\bar{a}_{Ga(C_2H_5)}}{\tau_2} \geq 0, \tag{30}$$

for $\bar{a}_{Ga(C_2H_5)}/\tau_2 \leq \bar{a}_{Ga(C_2H_5)_2}/\tau_1$. Fitting the initial decay of ΔR_N on the basis of $F_1(t_{d1})$ and $F_2(t_{d1})$ can be accomplished and can be extended in time by incorporating a time-dependent loss

$$a_{GaC_2H_5} = \left\{ \bar{a}_{Ga(C_2H_5)} + L(t) \bar{a}_{Ga(C_2H_5)_2} \right.$$

$$\times \left. \left[1 - \exp\left(-\frac{t}{\tau_1}\right) \right] \right\} \exp\left(-\frac{t}{\tau_2}\right) \tag{31}$$

with loss factor $L(t)$ starting from $L(t=0)=1$ and varying with same time dependence as $a_{GaC_2H_5}(t)$, corresponding to a maximum loss of 10% at the maximum in $F_2(t_{d1})$ for both experiments of Fig. 8. The curves labeled 1 and 2 in Figs. 8(a) and 8(b) are modeled with the same set of parameters $\tau_1 = 2.5$ s, $\tau_2 = 4.2$ s, $L(t)$, and $\bar{a}_{Ga(C_2H_5)} = 0.05 \times \bar{a}_{Ga(C_2H_5)_2}$. A possible interpretation of the loss of MEG is its parallel dealkylation through heterogeneous surface reactions at a rate that is tagged to the concentration of MEG in the homo-

geneous part of the SRL. The difference between the predicted behavior according to Eqs. (25) and (28) and the experimental data represented in Figs. 8(a) and 8(b) by the curves labeled 3 in the later stages of the decay of the SRL from its steady-state composition is attributed to surface reactions that become dominant as the TEG fragments become increasingly denuded of radical ligands. In this case, the dipole approximation is no longer a reliable basis for the evaluation of the dielectric function and no interpretation of these surface reactions can be offered on the basis of single pulse PR monitoring.

VI. SUMMARY AND CONCLUSIONS

On the basis of real-time process monitoring by *p*-polarized reflectance in combination with laser light scattering we have shown that, for a given flux of the phosphorus source vapor, there exists a narrow band of initial gallium supersaturations for the overgrowth of the silicon surface by a contiguous film of GaP with minimum roughening. Also, we have shown that steady-state heteroepitaxial growth must be represented by a four-layer stack: ambient–surface reaction layer–epilayer–substrate. Depending on the source vapor fluxes, the surface reaction layer can have a thickness of several monolayers of fragments of the gallium and phosphorus source vapor molecules. Based on the response in the PR intensity to variations and interruptions in the periodic source vapor pulse sequence—utilized for establishing steady-state conditions—we have show that the dealkylation of the gallium source molecules is the rate limiting step in the low temperature heteroepitaxial growth process. Its initial stages involving molecules and radicals that do not interact strongly with the underlying substrate can be modeled in terms of homogeneous reactions in the SRL. There exists at present no adequate description of the response in the PR intensity due to changes in the concentration of molecules and atoms bound directly to the surface atoms of the heteroepitaxial film. An assessment of the heterogeneous kinetics thus requires further research supplementing optical real-time process monitoring by additional methods of surface analysis.

[1] J. T. Kelliher, A. E. Miller, N. Dietz, S. Habermehl, Y. L. Chen, Z. Lu, G. Lucovsky, and K. J. Bachmann, Appl. Surf. Sci. **86**, 453 (1995).

[2] N. Dietz and K. J. Bachmann, MRS Bull. **20**, 49 (1995).

[3] D. E. Aspnes, J. P. Harbison, A. A. Studna, and L. T. Florez, J. Vac. Sci. Technol. A **6**, 1327 (1988).

[4] U. Rossow, N. Dietz and K. J. Bachmann, J. Vac. Sci. Technol. B **14**, 3040 (1996).

[5] J. Chadi, Phys. Rev. Lett. **59**, 1691 (1995).

[6] S. Miyoshi, H. Yaguchi, K. Onake, R. Ito, and Y. Shiraki, J. Cryst. Growth **145**, 87 (1994).

[7] H. Kroemer, J. Cryst. Growth **81**, 193 (1987).

[8] S-W Choi, K. J. Bachmann, T. Colpitts, J. B. Posthill, and M. L. Timmons, J. Electrochem. Soc. **139**, 312 (1992).

[9] W. A. Harrison, E. A. Kraut, J. R. Waldrop, and R. W. Kraut, Phys. Rev. B **18**, 4402 (1978).

[10] Y. Wang, M. J. Bonikowski, and R. J. Hamers, J. Phys. Chem. **98**, 5966 (1994).

[11] Y. Wang, X. Chen, and R. J. Hamers, Phys. Rev. B **50**, 4534 (1994).

[12] R. D. Bringans, M. A. Olmstead, R. I. G. Uhrberg, and R. Z. Bachrach, Phys. Rev. B **36**, 9569 (1987).

[13] G. S. Higashi, R. S. Becker, Y. J. Chabal, and A. J. Becker, Appl. Phys. Lett. **58**, 165 (1991).

[14] H. M'saad, J. Michel, A. Reddy, and L. C. Kimmerling, J. Electrochem. Soc. **142**, 2833 (1995).

[15] H. Angermann, K. Kliefoth, W. Füssel, and H. Flietner, Microelectron. Eng. **28**, 51 (1995).

[16] C. H. Bjorkman, J. L. Alay, H. Nishimura, M. Fukuda, T. Yamazaki, and M. Hirose, Appl. Phys. Lett. (to be published).

[17] Landolt-Börnstein, *Numerical Data and Functional Relationships in Science and Technology*, edited by O. Madelung and H. Weiss (Springer, Berlin, 1984), Vol. 17, p. 17.

[18] F. Ernst and P. Piroux, Appl. Phys. Lett. **64**, (1988).

[19] W. Kern, in *Current Topics of Materials Science*, edited by E. Kaldis (North-Holland, Amsterdam, 1979), Vol. 3, p. 131.

[20] C. H. Chen, C. A. Larsen, G. B. Stringfellow, D. W. Brown, and A. J. Robertson, J. Cryst. Growth **77**, 11 (1986).

[21] M. Grundmann, A. Krost, D. Bimberg, O. Ehrmann, and H. Cerva, Appl. Phys. Lett. **60**, 3292 (1992).

[22] M. Grundmann, J. Christen, F. Heinrichsdorf, A. Krost, and D. Bimberg, J. Electrochem. Soc. **23**, 201 (1994).

[23] A. Krost, R. F. Schabel, U. Rossow, D. Bimberg, and H. Cerva, J. Cryst. Growth **145**, 314 (1994).

[24] R. F. Schabel, A. Krost, M. Grundmann, D. Bimberg, and H. Cerva, J. Electron. Mater. **24**, 1625 (1995).

[25] S. Mahajan, K. J. Bachmann, D. Brasen, and E. Buehler, J. Appl. Phys. **49**, 245 (1978).

[26] A. E. Miller, N. Dietz, and K. J. Bachmann, Mater. Res. Soc. Symp. Proc. **355**, 197 (1995).

[27] K. J. Bachmann, N. Dietz, and U. Rossow, Mater. Sci. Eng. B **35**, 472 (1995).

[28] R. M. A. Azzam and N. M. Bashara, *Ellipsometry and Polarized Light* (North Holland, Amsterdam, 1987), p. 340.

[29] N. Dietz and K. J. Bachmann, Vacuum **47**, 133 (1996).

[30] S. H. Li, C. A. Larsen, N. I. Buchan, and G. B. Stringfellow, J. Appl. Phys. **65**, 5161 (1989).